The 2009 IEEE/RSJ International Conference on
Intelligent Robots and Systems
October 11-15, 2009 St. Louis, USA

Modeling and Parameter Identification of Rheological Object Based on FE Method and Nonlinear Optimization

Zhongkui Wang and Shinichi Hirai
Department of Robotics, Ritsumeikan University
Noji-higashi 1-1-1, Kusatsu, 525-8577, Japan
gr046074@ed.ritsumei.ac.jp, hirai@se.ritsumei.ac.jp

Abstract— **There are many kinds of deformable objects in our living life. Some of them such as human tissues, human organs, and food exhibit rheological behaviors when they are subject to external force. In surgery simulation and food engineering, we need to simulate or control such behaviors. In this paper, four-element model associated with finite element (FE) method was employed to model rheological deformation. This model can reach a good approximation of rheological force response when the object experience a standard strain input. An identification approach for estimating physical parameters of rheological deformation was presented based on 2D FE simulation and nonlinear optimization. This identification method aimed at minimizing the difference of force response between the simulation and experiment by using nonlinear least square method. Finally, experiments and identification results were given and both modeling and identification method were validated by comparing the results of simulation and experiments.**

I. INTRODUCTION

Along with the development of biomedical engineering, humanoid robot, and automation, people have to deal with more and more deformable objects. For example, robotic hands with soft finger surface to achieve more dexterous and stable grasp [1], surgical simulation by using soft tissue model [2], and shape control of soft object for food engineering [3], [4]. There are two important issues are involved for simulating deformable objects. The first one is modeling. An appropriate physical model has to be used to describe the deformation property, and then an appropriate modeling method must be chosen to compromise the requirement of accuracy and computation cost. The second issue is identification of physical parameters. For any physical model we used, there must be some unknown parameters which have to be available before simulating any real objects. Unfortunately, both modeling and parameter identification for rheological deformation are not well developed until now.

A. Related Works on Modeling

1) Physical Model: The well-known physical model for describing rheological deformation is three-element model [5], [6], [7], [8] which consists of two dampers and one spring. This is a linear model with minimal elements or physical parameters involved. Because the linear property, it is easy to extrapolate the constitutive law of stress and strain from one dimension to multi-dimensions. By using this physical model, we can obtain a good approximation of deformation, but the force approximation is not good enough. An explanation for the reason will be given in Section II. In addition, a few nonlinear physical models [9], [10] were proposed in recent years. These models can produce a good force curve fitting. But the application of these models was limited in only one dimensional deformation and it is difficult to extend to multi-dimensional cases.

2) Modeling Method: The modeling method of deformable objects has been studied intensively since late 80's and many methods had already been proposed, such as: the mass-spring-damper method (MSD) [11], the finite difference method (FDM) [12], the boundary element method (BEM) [13], and the finite element method (FEM) [14]. The computation cost and force accuracy increase in this order. Our previous work has developed an FE dynamic model for simulating rheological deformation based on three-element model[15].

B. Related Works on Parameter Identification

In recent years, some methods had already been proposed to estimate physical parameters of deformable objects. Most of them focus on elastic or viscoelastic deformation. One popular method is to iterate simulation with updated physical parameters. Material property is then obtained by minimizing the difference between displacements observed from images and calculated by simulations [16], [17]. However, they did not consider the force response during the optimization. So far, only few works can be found for parameters identification of rheological deformation and most of them employed MSD model [5], [6], [7], [18]. But none of them took inner deformation into account. In addition, our previous work [19] presented an approach to identify the physical parameters of rheological deformation based on 2D FE dynamic equations with three-element model.

In Section II, the four-element model is employed to model rheological deformation associated with FE method. In Section III, an identification method for estimating physical parameters is presented. Section IV gives some experiment and identification results. Section V shows a few conclusions and suggests future works.

II. MODELING

A. Analysis of Physical Model

Depending on the deformation behavior, soft objects can be roughly divided into three categories: viscoelastic, plastic, and rheological objects. Suppose that an object has a natural shape, as shown in Fig. 1(a). Applying external force, the

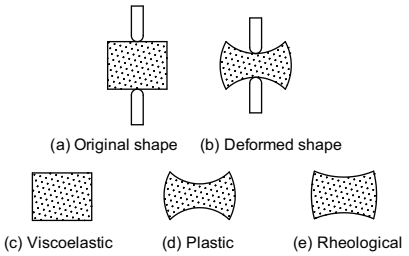

Fig. 1. Deformation classification of soft object

object deformed as shown in Fig. 1(b). After removing the force, viscoelastic objects totally turn back to the original shape, as shown in Fig. 1(c). Plastic objects maintain all the deformation and there is no recovered deformation, as shown in Fig. 1(d). However, rheological objects partially maintain the deformation but not all, as shown in Fig. 1(e).

From the description of rheological deformation, we know that rheological deformation has both elastic and viscous properties. The most simple and popular physical model for describing rheological deformation is the three-element model, as shown in Fig. 2(a), which is a serial connection of a Voigt model and a viscous element. As mentioned above, we can not obtain a good force approximation by using this model [19]. The constitutive law of stress and strain for this physical model can be compactly express as

$$\dot{\sigma} + a\sigma = b\ddot{\varepsilon} + c\dot{\varepsilon}, \tag{1}$$

where σ denotes the stress vector, ε denotes the strain vector, a, b, and c is three coefficients which are consist of three physical parameters E, c_1 and c_2. A typical force response of rheological deformation can be found in Fig. 2(b). The deformation procedure was divided into three phases. In the push phase ($0 - t_p$), the object was pushed with a constant velocity. In the keep phase, the deformation was kept for a time period ($t_p - t_p + t_k$). After time $t_p + t_k$, the external constraint was released and the deformation was recovered. In the keep phase, by substituting $\dot{\varepsilon} = 0$ and $\ddot{\varepsilon} = 0$ into (1) and solving it, we have $\sigma = \sigma(t_p)e^{-a(t-t_p)}$. Apparently, it is difficult to use this stress expression to approximate the force response in the keep phase as shown in Fig. 2(b). Because in this stress expression, there only include one exponential function and [10] suggests that we need at least two exponential functions to obtain a good approximation of force relaxation in the keep phase. For

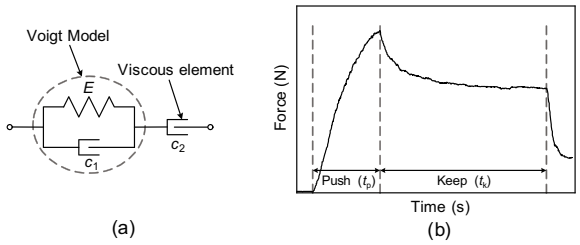

Fig. 2. (a) The three-element model. (b) Typical force response of rheological deformation

solving this problem, we introduce a four-element model by adding another spring element to three-element model to describe rheological deformation.

B. Four-element FE Model

By performing different connection between four elements, we can obtain several configurations of four-element model, as shown in Fig. 3. The last two models were called four-element Maxwell model [20] and Burgers fluid model [21] respectively. Fortunately, these four physical models have same constitutive law of stress and strain as below

$$\ddot{\sigma} + A_1\dot{\sigma} + A_0\sigma = B_1\ddot{\varepsilon} + B_0\dot{\varepsilon}, \tag{2}$$

where A_0, A_1, B_0, and B_1 are four coefficients which are decided by four physical parameters E_1, E_2, c_1 and c_2. The relationship between these coefficients and physical parameters can be found in Table I. From (2) we know that there includes second order time derivative of stress. So in the keep phase, if we substitute $\dot{\varepsilon} = 0$ and $\ddot{\varepsilon} = 0$ into (2) and solve it, we can yeild a stress expression with two exponential functions. It means this model can obtain a better force approximation than the three-element model.

Then, by using FE method, the stress-strain relationship can be converted into a relationship between a set of forces applied to nodal points and a set of displacements of the points. Let $\mathbf{u}_N$ be a set of displacements of nodal points. Let $\mathbf{J}_\lambda$ and $\mathbf{J}_\mu$ be connection matrices, which can be geometrically determined by coordinate components of nodal points. Furthermore, we define four pseudo Lamé's constants as follows:

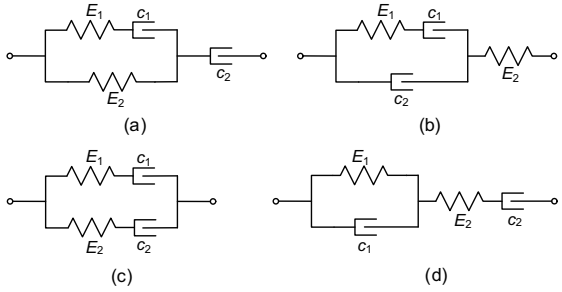

Fig. 3. Different configurations of four-element model

TABLE I
RELATIONSHIP BETWEEN COEFFICIENTS AND PARAMETERS

Model	A_0	A_1	B_0	B_1
(a)	$\frac{E_1E_2}{c_1c_2}$	$\frac{(E_1+E_2)c_1+E_1c_2}{c_1c_2}$	$\frac{E_1E_2}{c_1}$	E_1+E_2
(b)	$\frac{E_1E_2}{c_1c_2}$	$\frac{(E_1+E_2)c_1+E_1c_2}{c_1c_2}$	$\frac{E_1E_2}{c_1c_2}(c_1+c_2)$	E_2
(c)	$\frac{E_1E_2}{c_1c_2}$	$\frac{c_1E_2+c_2E_1}{c_1c_2}$	$\frac{E_1E_2}{c_1c_2}(c_1+c_2)$	E_1+E_2
(d)	$\frac{E_1E_2}{c_1c_2}$	$\frac{(E_1+E_2)c_2+E_2c_1}{c_1c_2}$	$\frac{E_1E_2}{c_1}$	E_2

$$B_0^\lambda = \frac{B_0\gamma}{(1+\gamma)(1-2\gamma)}, \quad B_0^\mu = \frac{B_0}{2(1+\gamma)},$$
$$B_1^\lambda = \frac{B_1\gamma}{(1+\gamma)(1-2\gamma)}, \quad B_1^\mu = \frac{B_1}{2(1+\gamma)}, \tag{3}$$

where γ is Poisson's ratio. For the sake of simplicity, we define two scalars m and n determined by A_0 and A_1 as below:

$$m = \frac{A_1 + \sqrt{A_1^2 - 4A_0}}{2}, \quad n = \frac{A_1 - \sqrt{A_1^2 - 4A_0}}{2}.$$

Then, a set of rheological forces applied to nodal points can be denoted by (4). A similar derivation can be found in [22].

$$\text{rheological force} = \mathbf{J}_\lambda(\omega_1^\lambda - \omega_2^\lambda) + \mathbf{J}_\mu(\omega_1^\mu - \omega_2^\mu), \tag{4}$$

where

$$\begin{aligned}
\omega_1^\lambda &= \frac{1}{m-n}\int_0^t e^{-n(t-t')}[B_0^\lambda \dot{\mathbf{u}}_N(t') + B_1^\lambda \ddot{\mathbf{u}}_N(t')]\mathrm{d}t', \\
\omega_1^\mu &= \frac{1}{m-n}\int_0^t e^{-n(t-t')}[B_0^\mu \dot{\mathbf{u}}_N(t') + B_1^\mu \ddot{\mathbf{u}}_N(t')]\mathrm{d}t', \\
\omega_2^\lambda &= \frac{1}{m-n}\int_0^t e^{-m(t-t')}[B_0^\lambda \dot{\mathbf{u}}_N(t') + B_1^\lambda \ddot{\mathbf{u}}_N(t')]\mathrm{d}t', \\
\omega_2^\mu &= \frac{1}{m-n}\int_0^t e^{-m(t-t')}[B_0^\mu \dot{\mathbf{u}}_N(t') + B_1^\mu \ddot{\mathbf{u}}_N(t')]\mathrm{d}t'.
\end{aligned} \tag{5}$$

Let $\mathbf{M}$ be an inertia matrix and $\mathbf{f}$ be a set of external forces applied to nodal points. Let us describe a set of geometric constraints imposed on the nodal points by $\mathbf{A}^\mathrm{T}\mathbf{u}_N = \mathbf{b}$. The number of columns of matrix $\mathbf{A}$ is equal to the number of geometric constraints. An elaborate definition of the constraint matrix can be found in [19]. Let λ be a set of constraint forces corresponding to the geometric constraints. A set of dynamic equations of nodal points is then given by

$$-\mathbf{J}_\lambda(\omega_1^\lambda - \omega_2^\lambda) - \mathbf{J}_\mu(\omega_1^\mu - \omega_2^\mu) + \mathbf{f} + \mathbf{A}\lambda - \mathbf{M}\ddot{\mathbf{u}}_N = 0.$$

Applying the constraint stabilization method (CSM) [23] to the constraints specified by constant angular velocity ω, system dynamic equations in 2D/3D case can be then formulated as follows:

$$\begin{aligned}
\dot{\mathbf{u}}_N &= \mathbf{v}_N, \\
\mathbf{M}\dot{\mathbf{v}}_N - \mathbf{A}\lambda &= -\mathbf{J}_\lambda(\omega_1^\lambda - \omega_2^\lambda) - \mathbf{J}_\mu(\omega_1^\mu - \omega_2^\mu) + \mathbf{f}, \\
-\mathbf{A}^\mathrm{T}\dot{\mathbf{v}}_N &= \mathbf{A}^\mathrm{T}(2\omega\mathbf{v}_N + \omega^2\mathbf{u}_N), \\
-\frac{B_1^\lambda}{m-n}\dot{\mathbf{v}}_N + \dot{\omega}_1^\lambda &= -n\omega_1^\lambda + \frac{B_0^\lambda}{m-n}\mathbf{v}_N, \\
-\frac{B_1^\mu}{m-n}\dot{\mathbf{v}}_N + \dot{\omega}_1^\mu &= -n\omega_1^\mu + \frac{B_0^\mu}{m-n}\mathbf{v}_N, \\
-\frac{B_1^\lambda}{m-n}\dot{\mathbf{v}}_N + \dot{\omega}_2^\lambda &= -m\omega_2^\lambda + \frac{B_0^\lambda}{m-n}\mathbf{v}_N, \\
-\frac{B_1^\mu}{m-n}\dot{\mathbf{v}}_N + \dot{\omega}_2^\mu &= -m\omega_2^\mu + \frac{B_0^\mu}{m-n}\mathbf{v}_N.
\end{aligned} \tag{6}$$

By using numerical solver such as the Euler method or the Runge-Kutta method to solve above differential equations, we can finally sketch $\mathbf{u}_N$, $\mathbf{v}_N$, ω_1^λ, ω_1^μ, ω_2^λ, and ω_2^μ.

III. PARAMETER IDENTIFICATION

In this section, we shall introduce an approach to identify physical parameters of rheological deformation based on FE simulation and nonlinear optimization. First of all, let us see how these physical parameters and mesh distribution will effect deformation behavior and force response during simulation.

A. Simulation Analysis

Now, let us apply the dynamic model of rheological deformation to a rectangular object with width=80mm, height=80mm, and thickness=12.5mm. We suppose this is a 2D deformation and the object surface was divided into 32 triangles with 25 nodal points. A four-element model (here we choose model (b) in Fig. 3) is attached on each triangle. The bottom surface of object is fixed on the ground. From time 0s to 20s, the top surface of object is pushed down with a constant velocity of 0.5mm/s. Then, the deformation is kept constant from time 20s to 60s. If we suppose the deformation is isotropic and homogeneous, the deformation and force response are decided by 5 physical parameters: E_1, E_2, c_1, c_2, and γ. However, the contributions of these parameters are different to the consequential deformation and force response.

1) Contribution of Poisson's Ratio: Let us consider simulations with different Poisson's ratios: $\gamma = 0.25$, $\gamma = 0.35$, and $\gamma = 0.45$. Other four parameters are unchanged with values of $E_1 = 5\times10^2$, $E_2 = 1.2\times10^3$, $c_1 = 2\times10^4$, and $c_2 = 8\times10^3$. The deformation and force response are shown in Fig. 4. From Fig. 4 we know that the Poisson's ratio γ effects both deformation and force response.

2) Contribution of Elastic Modulus: Let us compare simulation results with different elastic moduli. Fig. 5(a) and (b) show the deformation behavior and force response with different E_1 and (c) and (d) correspond to E_2. From Fig. 5 we know that elastic moduli only contribute to force response, they do not effect the deformed shape (during keep phase) at all.

3) Contribution of Viscous Modulus: Now, let us perform the same comparison with different viscous moduli, as shown in Fig. 6. Here we only give the force response with variational c_1 and c_2 because the deformation behaviors are same with Fig. 5(a) and (c). Fig. 6 indicates that the viscous moduli also only effect force response.

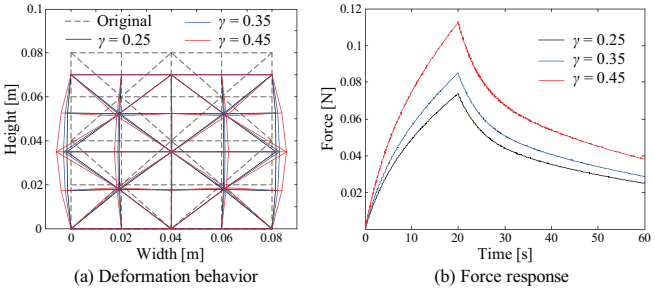

(a) Deformation behavior (b) Force response

Fig. 4. Simulation results with different Poisson's ratio γ.

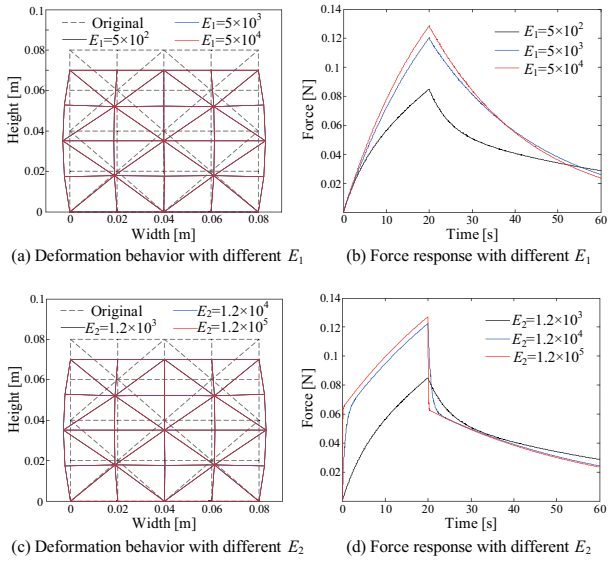

(a) Deformation behavior with different E_1 (b) Force response with different E_1

(c) Deformation behavior with different E_2 (d) Force response with different E_2

Fig. 5. Simulation results with different elastic moduli E_1 and E_2.

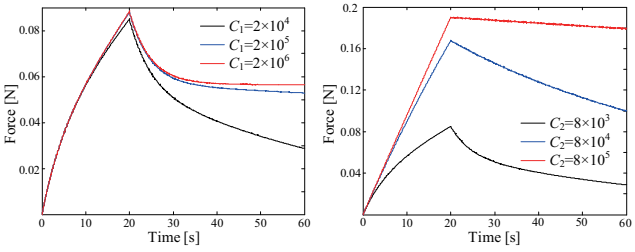

(a) Force response with different c_1 (b) Force response with different c_2

Fig. 6. Simulation results with different viscous moduli c_1 and c_2.

In addition, mesh distribution also effects simulation results. A rule of thumb is that the finer the mesh is distributed, the higher the accuracy of simulation results will be. Fig. 7 shows how the mesh distributions effect simulation results. According to Fig. 7, we know that the discrepancy of both deformation and force response between different mesh distributions is not significant if the mesh distribution is finer than 4×4 in this simple deformation.

B. Optimization Process for Identification

We have totally five physical parameters in 2D/3D deformation: E_1, E_2, c_1, c_2, and γ. However, from the simulation analysis presented in last subsection we know that only Poisson's ratio γ effects deformed shapes, the other four parameters only contribute to force response. This means we can separately identify the Poisson's ratio by minimizing the difference of deformation between simulation and experiment. For a commercial clay which will be used in our experiment, [19] had already given a value of $\gamma = 0.332$ and worked well for approximating the deformation behavior. So, in this paper, we focus on the other four physical parameters and we assume Poisson's ratio $\gamma = 0.35$.

Fig. 8 shows the optimization process of parameter identification. We assign the initial estimation of physical parameters to the 2D dynamic model, and repeat the FE simulation

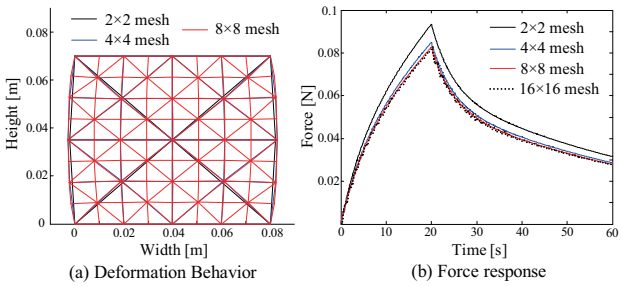

(a) Deformation Behavior (b) Force response

Fig. 7. Simulation results with different mesh distributions.

with updated physical parameters until the difference between the force data measured in experiment and calculated by FE simulation is minimized. The objective function of this problem can be described as follows:

$$F(x) = \frac{1}{2}\sum_{i=1}^{m}\left[f^{sim}(x,t_i) - f^{exp}(t_i)\right]^2, \tag{7}$$

where x is the physical parameters, t_1 through t_m are times to be sampled, $f^{sim}(x,t_i)$ is the calculated force output by simulation when the physical parameters are x and sampling time is t_i, and $f^{exp}(t_i)$ is the measured force data at sampling time t_i.

Then, a 'nonlinear least squares' method with 'large-scale: trust-region reflective Newton' algorithm is employed to minimize the objective function. This nonlinear optimization method is widely used in data fitting problems.

IV. EXPERIMENT RESULTS

A. Pushing Experiment

The commercial clay made of flour, water, and salt was employed to work as a rheological object through our experiments. The object of size about 80mm × 80mm × 12.5mm was pushed by a motorized stage with a displacement about 9.6mm and a constant velocity of 0.5mm/s (t_p=19.21s). Before releasing, the displacement was kept about 47.88 seconds (t_k). Some markers were drawn on the surface of the clay by using a resist pen filled with lacquer ink. The initial and deformed shapes recorded by a camera are shown in Fig. 9(a), (b), and (c). By using a simple image processing, we can obtain a 2D FE mesh of these shapes as shown in Fig. 9(d), (e), and (f). The force data recorded by a tactile sensor can be found in Fig. 2(b).

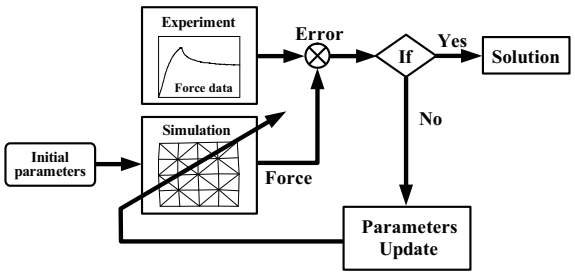

Fig. 8. Optimization process for parameter identification.

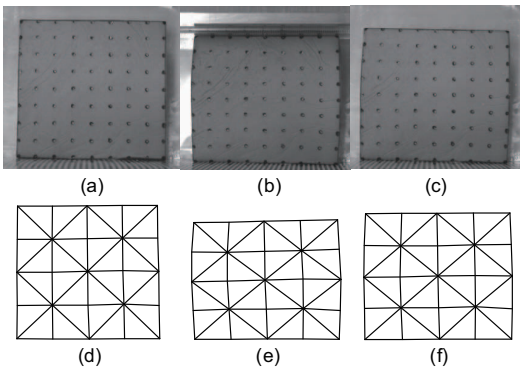

Fig. 9. Deformation behaviors in experiment. (a), (b), (c): Images taken by camera. (d), (e), (f): Description of images by using 2D mesh. (a), (d): Initial shape. (b), (e): Deformed shape in the end of keep phase. (c), (f): Final shape after releasing.

TABLE II

INITIAL VALUE AND IDENTIFIED VALUE OF PHYSICAL PARAMETERS

Parameters	Initial Value x_0	Identified Value x^*
E_1 (Pa)	3×10^4	5.8388×10^4
E_2 (Pa)	5×10^3	1.2353×10^5
c_1 (Pa·s)	2×10^5	2.1091×10^7
c_2 (Pa·s)	6×10^5	8.3402×10^5

B. Identification Results

During the optimization process, we choose to use the physical model (b) shown in Fig. 3 with a 4×4 mesh distribution. After 74 iterations and 375 times FE simulations, the optimization analysis terminated because the relative function value changing is less than 1×10^{-6}. The objective function finally converged to a value of 1.9261N. The initial value and identified value of physical parameters are shown in Table II. By performing some simple calculations, one can obtain these parameters for other physical models (shown in Fig. 3(a), (c), and (d)) based on Table I.

Furthermore, let us compare the deformation behavior and force response between the simulation results and experiment results, as shown in Fig. 10. We can see from Fig. 10 that we can obtain good approximation for both deformation behavior and force response.

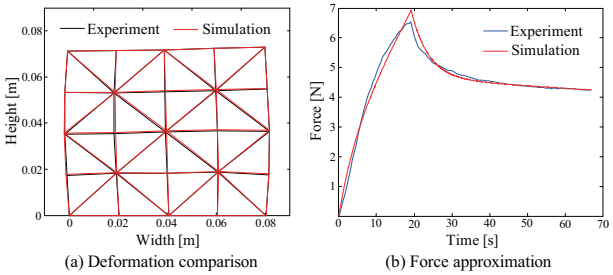

(a) Deformation comparison (b) Force approximation

Fig. 10. Deformation comparison and force approximation for the first experiment.

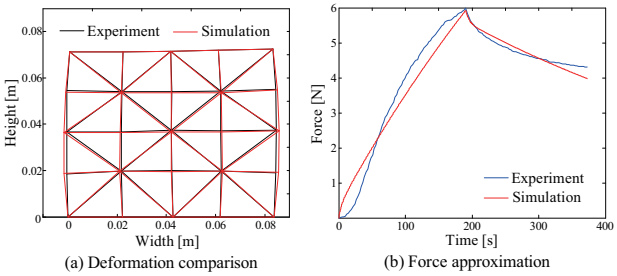

(a) Deformation comparison (b) Force approximation

Fig. 11. Deformation comparison and force approximation for the second experiment.

In order to validate our identification results, we conduct another experiment with the same material. This time we pushed the object slower and kept the deformation longer than the first experiment, here t_p=190.72s and t_k=182.37s. Then, we use the physical parameters given in Table II to simulate this deformation behavior and force response. A comparison between simulation results and experiment results are shown in Fig. 11.

As we mentioned in Section III, the mesh distributions effect force response. Now let us check the influence of mesh distributions in both experiments. Here we only give the comparison of force response in Fig. 12. The deformation comparison is similar with Fig. 7(a). According to Fig. 12, we believe that in this simple deformation behavior, 4×4 mesh distribution is accurate enough to describe both deformation and force.

The deformed shapes showed in Fig. 10(a) and Fig. 11(a) are in the end of keep phase. Now let us consider the final shape after releasing the external constraints. Deformation comparison of final shape for both experiments are shown

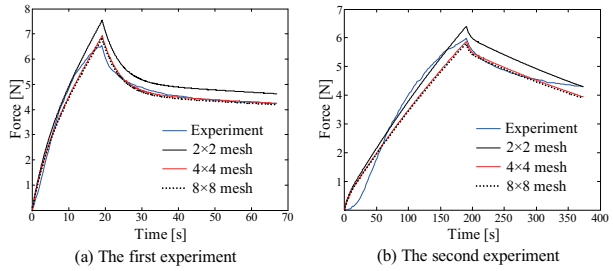

(a) The first experiment (b) The second experiment

Fig. 12. Force approximation with different mesh distribution for both experiments.

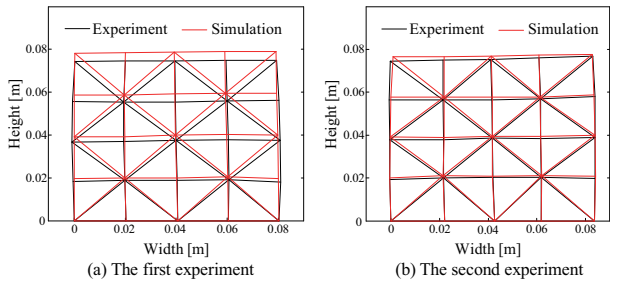

(a) The first experiment (b) The second experiment

Fig. 13. Deformation comparison of final station for both experiments.

in Fig. 13. This figure means that we could not obtain a good approximation for final shape. It is because that the deformation behavior after releasing external constraint depends not only on Poisson's ratios γ, but also on other four physical parameters. However, during our optimization process, we did not take the final shape into account. Another reason probably is because the four-element model we used in this paper still linear model and the 2D dynamic model used to simulate rheological deformation is based on this physical model. This can explain why the discrepancy of final shape in the second experiment(as shown in Fig. 13(b)) is smaller than the first experiment (as shown in Fig. 13(a)). It is because that the slower the object is pushed and the longer the deformation is kept, the smaller the dynamic influence will be.

V. CONCLUSIONS AND FUTURE WORKS

In this paper, we introduced four-element model associated with FE method to model rheological deformation. 2D/3D FE dynamic equations were presented. According to the simulation analysis, we found out that only Poisson's ratio γ effects the deformed shape when the object is subjected to a displacement constraint. Other four physical parameters E_1, E_2, c_1, and c_2 only effect force response during push and keep phase. Then, an approach was proposed to identify these four physical parameters based on FE simulation and nonlinear optimization. The FE simulation was repeated with updated physical parameters until the difference between the force data measured in experiment and calculated by FE simulation was minimized. This identification method needs less measured data compare with our last method [19]. We only need to measure force response on a surface, an area or even one point and displacements of some nodal points. Finally, experiments and identification results were given and the comparisons of deformation and force response between simulations and experiments validated both our model and identification method.

In our future works, the Poisson's ratio γ and deformation information will be taken into account during the optimization process to yield a multi-objective optimization problem. Nonlinear behavior will be explored to obtain a more accurate rheological model. In addition, both FE model and identification method will be extended and applied to non-uniform rheological deformation.

REFERENCES

[1] R. W. Brockett, "Robotic Hands with Rheological Surfaces", *in Proc. of the 1985 IEEE International Conference on Robotics and Automation*, St. Louis, 1985, pp. 942-946.

[2] I. Brouwer, V. Mora, D. Laroche, "A Viscoelastic Soft Tissue Model for Haptic Surgical Simulation", *in EuroHaptics Conference, 2007 and Symposium on Haptic Interfaces for Virtual Environment and Teleoperator Systems*, Tsukaba, 2007, pp. 593-594.

[3] S. Tokumot, Y. Fujita, S. Hirai, "Deformation Modeling of Viscoelastic Objects for Their Shape Control", *in Proc. of the 1999 IEEE International Conference on Robotics and Automation*, Detriot, 1999, pp. 767-772.

[4] M. Kimura, Y. Sugiyama, S. Tomokuni, S. Hirai, "Constructing Rheologically Deformable Virtual Objects", *in Proc. of the 2003 IEEE International Conference on Robotics and Automation*, Taipei, 2003, pp. 3737-3743.

[5] H. Noborio, R. Enoki, S. Nishimoto, T. Tanemura, "On the Calibration of Deformation Model of Rheology Object by a Modified Randomized Algorithm", *in Proc. of the 2003 IEEE International Conference on Robotics and Automation*, Taipei, 2003, pp. 3729-3736.

[6] R. Nogami, H. Noborio, F. Ujibe, H. Fujii, "Precise Deformation of Rheologic Object under MSD Models with Many Voxels and Calibrating Parameters", *in Proc. of the 2004 IEEE International Conference on Robotics and Automation*, New Orleans, 2004, pp. 1919-1926.

[7] H. Yoshida, Y. Murata, H. Noborio, "A Smart Rheologica MSD Model Pushed/Calibrated/Evaluated by Experimental Impulses", *in IEEE/RSJ International Conference on Intelligent Robots and Systems*, Edmonton, 2005, pp. 269-276.

[8] T. Ikawa, H. Noborio, "On the Precision and Efficiency of Hierarchical Rheology MSD Model", *in IEEE/RSJ International Conference on Intelligent Robots and Systems*, San Diego, 2007, pp. 376-283.

[9] L. Bitman, Y. T. Choi, S. B. Choi, N. M. Wereley, Electrorheological Damper Analysis Using an Eyring-plastic Model, *Smart Materials and Structures*, vol. 14(1), 2005, pp. 237-246(10).

[10] C. D. Tsai, I. Kao, N. Sakamoto, M. Higashimori, M. Kaneko, "Applying Viscoelastic Contact Modeling to Grasping Task: an Experimental Case Study", *in IEEE/RSJ International Conference on Intelligent Robots and Systems*, Nice, 2008, pp. 1790-1795.

[11] K. Waters, "A Muscle Model for Animating Three-dimensional Facial Expression", *in Proc. of the 14th Annual Conference on Computer Graphics and Interactive Techniques*, Anaheim, 1987, pp. 17-24.

[12] D. Terzopoulos, J. Platt, A. Barr, K. Fleischer, "Elastically Deformable models", *in Proc. of the 14th Annual Conference on Computer Graphics and Interactive Techniques*, Anaheim, 1987, pp. 205-214.

[13] D. L. james, D. K. Pai, "Artdefo: Accurate Real Time Deformable Objects", *in Proc. of the 26th Annual Conference on Computer Graphics and Interactive Techniques*, Los Angeles, 1999, pp. 65-72.

[14] M. B. Nielsen, S. Cotin, "Real-time Volumetric Deformable Models for Surgery Simulation Using Finite Elements and Condensation", *in Computer Graphics Forum (Proc. Eurographics'96)*, Poitiers, 1996, pp. 57-66.

[15] J. Muramatsu, T. Ikuta, S. Hirai, "Validation of FE Deformation Models Using Ultrasonic and MR Images", *in Proc. of the 9th International Conference on Control, Automation, Robotics and Vision*, Singapore, 2006, pp. 1-6.

[16] T. Hoshi, Y. Kobayashi, K. Kawamura, M. G. Fujie, "Developing an Intra-operative Methodology Using the Finite Element Method and the Extended Kalman Filter to Identify the Material Parameters of an Organ Model", *in Proc. of the 29th Annual Interational Conference of the IEEE EMBS*, Lyon, 2007, pp. 469-474.

[17] M. Tada, N. Nagai, T. Maeno, Material Properties Estimation of Layered Soft Tissue Based on MR Observation and Iterative FE Simulation, *Medical Image Computing and Computer-Assisted Intervention*, vol. 3750, 2005, pp. 633-640.

[18] N. Ueda, S. Hirai, H. T. Tanaka, "Extracting Rheological Properties of Deformable Objects with Haptic Vision", *in Proc. of the 2004 IEEE International Conference on Robotics and Automation*, New Orleans, 2004, pp. 3902-3907.

[19] Z. K. Wang, K. Namima, S. Hirai, "Physical Parameter Identification of Rheological Object Based on Measurement of Deformation and Force", *in Proc. of the 2009 IEEE International Conference on Robotics and Automation*, Kobe, 2009, pp. 1238-1243.

[20] N. Sakamoto, M. Higashimori, T. Tsuji, M. Kaneko, "An Optimum Design of Robotic Hand for Handling a Visco-elastic Object Based on Maxwell Model", *in Proc. of the 2007 IEEE International Conference on Robotics and Automation*, Roma, 2007, pp. 1219-1225.

[21] I. H. Shames, F. A. Cozzarelli, *Elastic and Inelastic Stress Analysis*, New Jersey: Englewood, 1992, ch. 6.

[22] S. Hirai, S. Tomokuni, "Dynamic Modeling of Rheological Deformation", *in Proc. of the 2004 JSME Conference on Robotics and Mechatronics Division*, Nagoya, 2004, pp. 2A1-H-7.

[23] J. Baumgarte, Stabilization of Constraints and Integrals of Motion in Dynamical Systems, *Computer Methods in Applied Mechanics and Engineering*, vol. 1, 1972, pp. 1-16.